JOURNAL OF VIROLOGY, Oct. 2004, p. 11416–11421 Vol. 78, No. 20
0022-538X/04/$08.00+0 DOI: 10.1128/JVI.78.20.11416–11421.2004

Resolution of Primary Severe Acute Respiratory Syndrome-Associated Coronavirus Infection Requires Stat1

Robert J. Hogan,[1] Guangping Gao,[2] Thomas Rowe,[1] Peter Bell,[2] Douglas Flieder,[3] Jason Paragas,[4] Gary P. Kobinger,[2] Nelson A. Wivel,[2] Ronald G. Crystal,[5] Julie Boyer,[5] Heinz Feldmann,[6] Thomas G. Voss,[1] and James M. Wilson[2]*

Department of Homeland Security, Southern Research Institute, Birmingham, Alabama[1]; Gene Therapy Program, Division of Medical Genetics, Department of Medicine, University of Pennsylvania, Philadelphia, Pennsylvania[2]; Department of Pathology[3] and Department of Genetic Medicine,[5] Weill Medical College of Cornell University, New York, New York; United States Army Medical Research Institute of Infectious Diseases, Frederick, Maryland[4]; and Department of Medical Microbiology, University of Manitoba and National Microbiology Laboratory, Winnipeg, Canada[6]

Received 2 April 2004/Accepted 28 May 2004

Intranasal inhalation of the severe acute respiratory syndrome coronavirus (SARS CoV) in the immunocompetent mouse strain 129SvEv resulted in infection of conducting airway epithelial cells followed by rapid clearance of virus from the lungs and the development of self-limited bronchiolitis. Animals resistant to the effects of interferons by virtue of a deficiency in Stat1 demonstrated a markedly different course following intranasal inhalation of SARS CoV, one characterized by replication of virus in lungs and progressively worsening pulmonary disease with inflammation of small airways and alveoli and systemic spread of the virus to livers and spleens.

The presentation of humans with severe acute respiratory syndrome (SARS) in several regions of Asia and Canada recently led to the isolation of related strains of a novel coronavirus (7, 10). Epidemiologic studies strongly suggest that these new coronaviruses (called SARS coronaviruses, or SARS CoV) are the causative agents of SARS (7, 10). This report describes the use of mouse models to study the pathogenesis of SARS CoV infection with respect to Stat1-dependent host responses.

Stat1$^{-/-}$ mice and the parental strain (129SvEv) were infected with SARS CoV of the Toronto-2 strain via intranasal inhalation (6×10^6 PFU/30 μl). Animals were necropsied 1, 3, 5, 8, 11, 15, and 22 days after SARS CoV challenge. Livers, spleens, and lungs were either homogenized and evaluated for the presence of SARS CoV by PFU assay and SARS CoV genomes by TaqMan reverse transcription (RT)-PCR or fixed in formalin and analyzed for histopathology and expression of SARS CoV antigens by immunohistochemistry. Animals were also monitored for clinical sequelae through direct observation and measurement of body weights.

SARS CoV and SARS CoV genomes were detected at equivalent levels in both strains of mice 1 day after administration, although the subsequent kinetics of virus replication evolved very differently in 129SvEv (Fig. 1A) and Stat1$^{-/-}$ (Fig. 1B) mice. Virus was rapidly cleared from lungs of 129SvEv mice to undetectable levels by day 8. Levels of viral genomes increased slightly in lungs of 129SvEv mice between days 1 and 3 and thereafter declined with kinetics similar to those of the virus. Livers and spleens harbored low levels of viral genomes in 129SvEv mice soon after infection; a few animals demonstrated an increase in levels of viral genomes in lungs, spleens, and livers at the day-22 time point. Replication of SARS CoV was clearly demonstrated in lungs of Stat1$^{-/-}$ mice, with increases in levels of virus and viral genomes of 2 logs in lungs of Stat1$^{-/-}$ mice between days 1 and 3. In these mice, substantial levels of lung-associated SARS CoV genomes persisted without diminution between days 5 and 22. Numbers of viral genomes associated with spleens and livers rapidly increased from 100 genomes/μg of RNA at day 1 to 10^5 to 10^6 genomes/μg of RNA at day 22 in all Stat1$^{-/-}$ animals. To determine whether these genomes were transcriptionally active, total RNA was analyzed for the formation of subgenomic transcripts by using a PCR strategy (Fig. 1C) (13). Tissues that were positive for SARS CoV RNA by TaqMan PCR showed formation of the nucleoprotein subgenomic mRNA, indicating the presence of transcriptionally active SARS CoV genomes (Fig. 1D).

Tissues were harvested and analyzed for evidence of pathology and cellular distribution of SARS CoV infection. Immunohistochemical analyses using a pool of polyclonal antibodies to spike protein revealed epithelial cells of noncartilaginous conducting airways (i.e., bronchioles) as the primary site of SARS CoV infection immediately following virus administration in both strains of mice (Fig. 2A and B). Immunofluorescence staining with confocal imaging revealed two patterns: subcellular localization of spike protein in epithelial cells of conducting airways as focal intracellular aggregates, a pattern which is consistent with the formation of virus in pre-Golgi compartments (Fig. 3A) (6, 11, 14), and diffuse distribution throughout the cytoplasm (Fig. 3B).

SARS CoV infection resulted in self-limited bronchiolitis in 129SvEv mice. Mixed inflammatory infiltrates initially surrounded bronchioles (Fig. 4A). Over the ensuing 5 days, these lesions evolved to include bronchiolitis with migration of in-

* Corresponding author. Mailing address: 204 Wistar, 3601 Spruce St., Philadelphia, PA 19104. Phone: (215) 898-0819. Fax: (215) 898-6588. E-mail: wilsonjm@mail.med.upenn.edu.

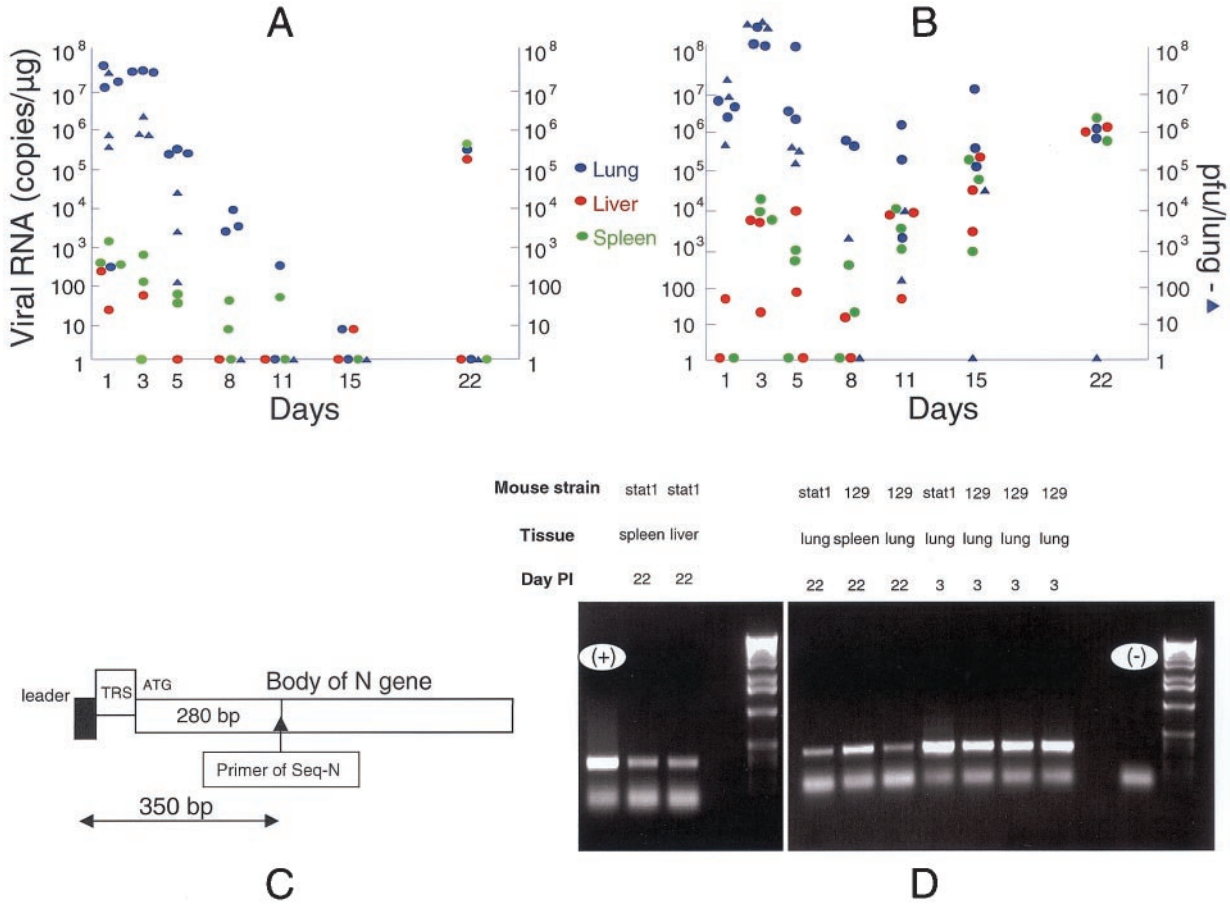

FIG. 1. 129SvEv (A) and Stat1$^{-/-}$ (B) mice were infected with SARS CoV, and tissues were harvested, homogenized, and analyzed for levels of SARS CoV by using a limiting-dilution plaque assay (i.e., PFU) on Vero E6 cells and for levels of SARS CoV genomes by using TaqMan RT-PCR. Stat1$^{-/-}$ mice were initially generated by Meraz et al. (8) by mating the original chimera directly to a 129SvEv mouse to produce 129SvEv heterozygotes which were intercrossed to obtain the desired homozygotes on a pure 129SvEv background. The animals were purchased from Taconic Animal Models. The Toronto-2 strain of SARS CoV was initially isolated in Canada from a human patient with a fatal case of SARS; the stock used for infection was a third passage recovered from supernatants of infected Vero E6 cells (titer = 1.2×10^8 PFU/ml). One microgram of total-tissue RNA was reverse transcribed using the high-capacity cDNA archive kit (Applied Biosystems, Foster City, Calif.) by following the manufacturer's instructions. Crude SARS CoV RNA that was extracted from infected Vero E6 cells served as a control in each RT-PCR run. For the real-time PCRs, primer and probe sets were designed to target the N gene of the SARS CoV. The restriction fragment of the N gene isolated from a plasmid construct was serially diluted and used as a template to establish the standard curves. One-tenth of each RT reaction mixture was used in TaqMan PCRs, which were carried out on an ABI PRISM 7700 sequence detector (Applied Biosystems). Each data point represents the result from a separate animal. Recovery of virus is presented as numbers of PFU per lung and is represented by blue triangles, and viral genome levels are presented as numbers of copies per microgram of total RNA for lungs, livers, and spleens. Animals were harvested at the indicated times. (C and D) Analysis of total cellular RNA for the presence of the subgenomic mRNA encoding nucleoprotein. The strategy was to amplify RNA by PCR using probes specific to the leader and nucleoprotein sequences. If the nascent RNA was processed into a subgenomic transcript, the PCR should yield a band of approximately 350 bp in length (C). One microgram of each total-tissue RNA was diluted in water in a final volume of 50 μl, and the RNA was reverse transcribed using the high-capacity cDNA archive kit (Applied Biosystems) in a 100-μl reaction mixture. RNAsecure (Ambion, Austin, Tex.) was added to the RT reaction mixtures to ensure the inactivation of RNase in solutions. The RT reaction was carried out in the GeneAmp PCR System 9600 thermal cycler in two incubation steps, an initial 25°C incubation for 10 min followed by a final 37°C incubation for 2 h. A no-reverse transcriptase control was included in the RT reactions. For the PCR step, two primers were designed to target the common leader sequence region (PCR-L, 5′ GGAAAAGCCAACCAACCTCGATCTC 3′) and the body sequence (PCR-N, 5′ TCGGGTAGCTCTT CGGT AGTAGCC 3′) of the N gene open reading frame. The N gene-specific sequence in the PCR amplicon is 280 bp in length. Since there is no published sequence for the transcript between the leader sequence and the start codon of subgenomic mRNA for the N gene, we estimated that the entire amplicon should be 300 to 400 bp by using the two primers described above. (D) An aliquot of each RT reaction mixture (5 μl) from 11 samples (input virus control, input virus control without reverse transcriptase, three day-3 lung samples from three 129SvEv [129] mice, day-22 lung and spleen samples from one 129SvEv mouse each, a day-3 lung sample from one Stat1$^{-/-}$ [stat1] mouse, and day-22 lung, liver, and spleen samples from one Stat1$^{-/-}$ mouse) was subjected to PCR in 25-μl reaction mixtures under the standard PCR conditions. Ten microliters each of PCR products was electrophoresed on a 1.2% agarose gel and visualized by ethidium bromide staining. TRS, transcription regulatory sequence; Seq-N, SARS virus N gene sequence; PI, postinoculation.

flammatory cells into the surface epithelia and sloughing of epithelial cells (Fig. 4B) as well as interstitial inflammation in adjacent alveolar septa (Fig. 4C). Immunohistochemistry with cell-specific markers indicated that many of the peribronchiolar inflammatory cells were macrophages (data not shown). Over the next 2 weeks, the bronchiolitis and patchy interstitial pneumonia completely resolved (Fig. 4D). The 129SvEv mice showed no abnormal clinical findings (data not shown). The

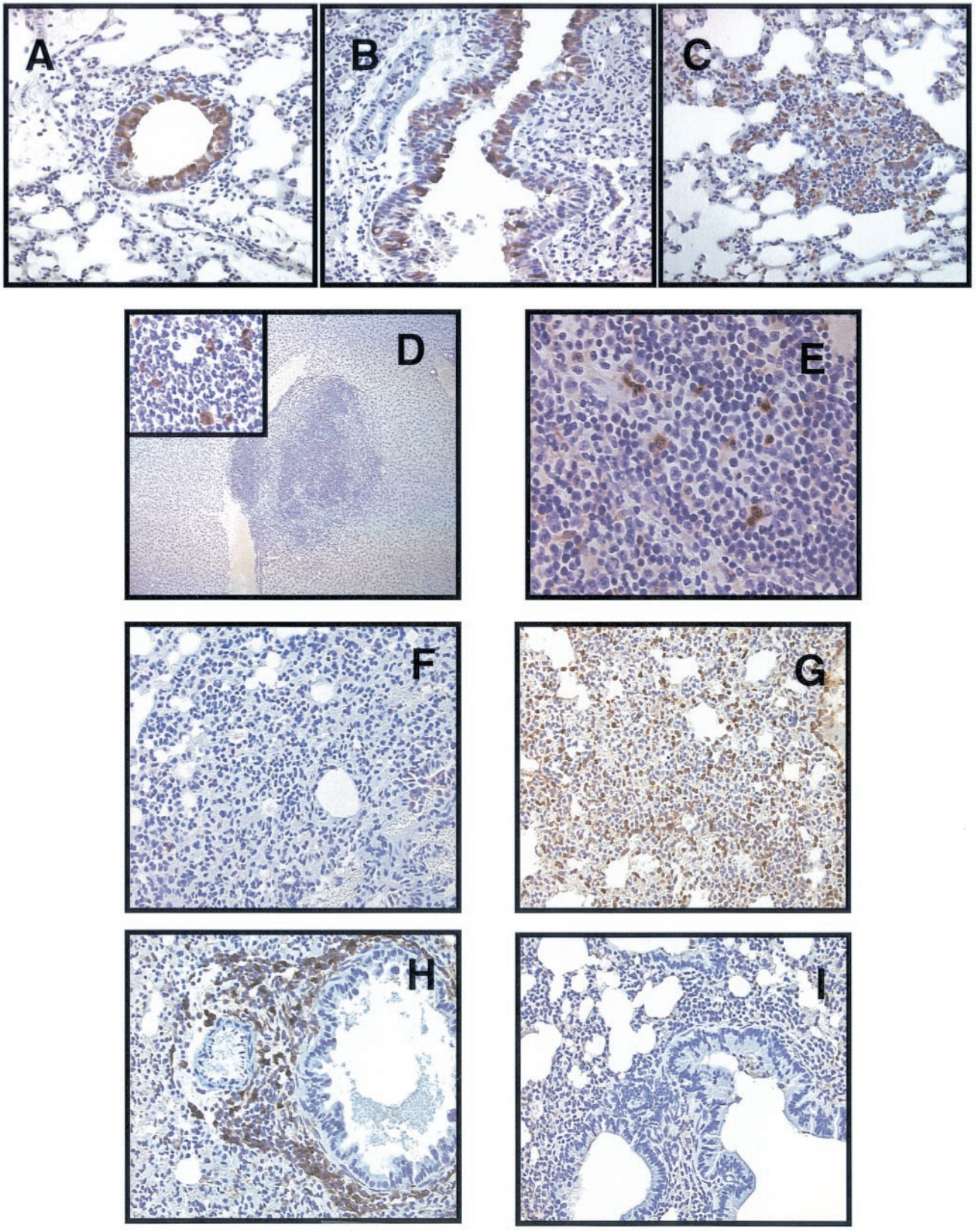

FIG. 2. Immunohistochemical analysis of SARS CoV infections. Tissues were harvested from Stat1$^{-/-}$ mice and analyzed for expression of SARS CoV antigens (A to E) and markers of inflammatory cells (F to I) by immunohistochemistry. Several antisera were used that were directed against the spike and nucleocapsid proteins on sections from paraffin-embedded tissues, including commercial antibodies (from Imgenex and Abgent) and rabbit sera made in our laboratory. Best results were obtained with a mix of six of our rabbit sera raised against spike. Antisera used

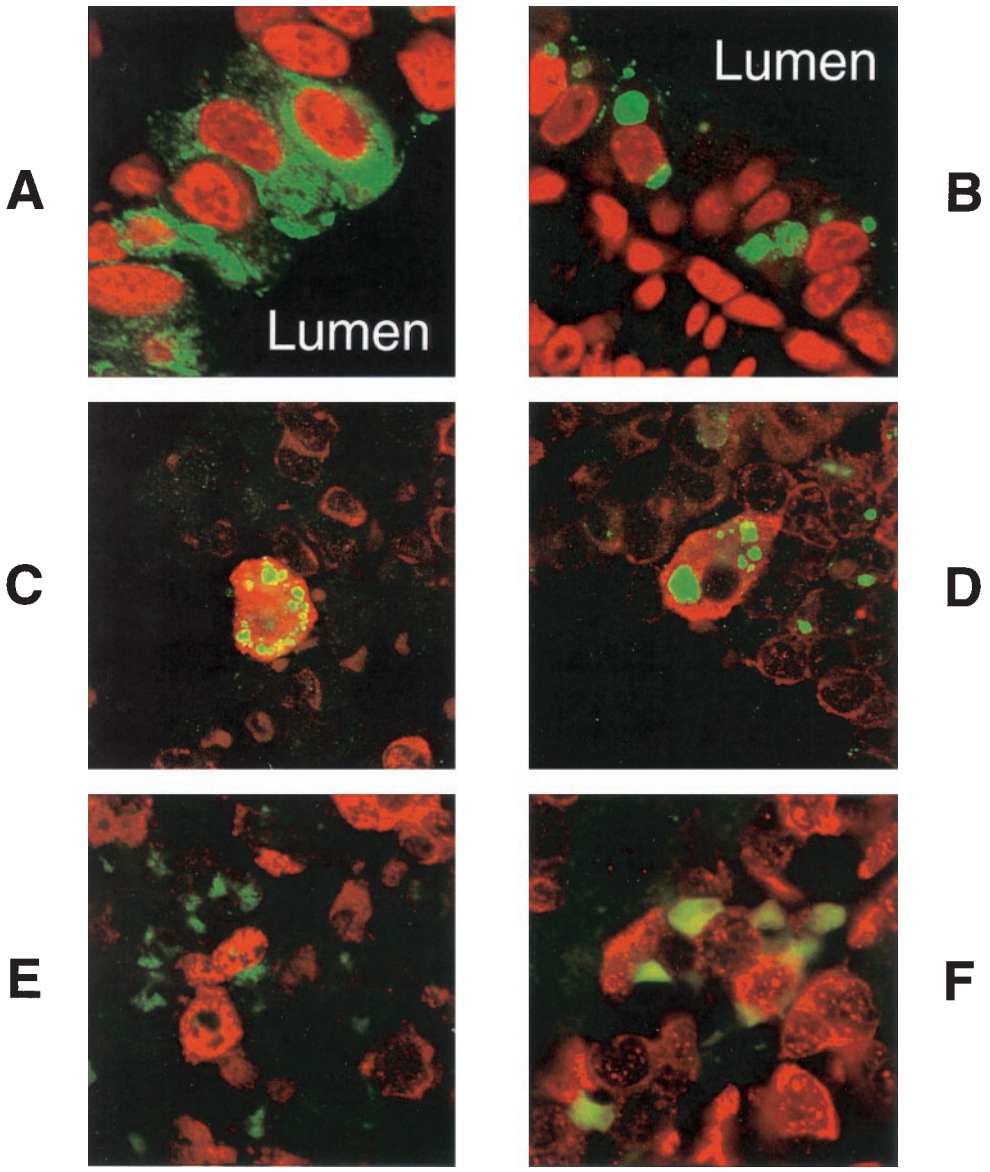

FIG. 3. Immunofluorescent analysis of spike expression in lung and liver. Tissues harvested from Stat1$^{-/-}$ mice at various time points after SARS CoV challenge were analyzed for spike expression as indicated. (A and B) Spike expression (green) in epithelial cells of the conducting airways with propidium iodide used to illustrate nuclei (red) from lungs of Stat1$^{-/-}$ mice harvested on day 3 after challenge. Lumens of airways are indicated. (C and D) Results of double immunofluorescence studies using antibodies to spike (green) and the macrophage marker Mac-2 (red) from lungs harvested 30 days after challenge. (E and F) Similar analyses for livers harvested from Stat1$^{-/-}$ mice 22 days after challenge by using antibodies against F4/80 antigen (panel E; red) and Mac-2 (panel F; red) to visualize macrophages (spike is in green). Similar findings were demonstrated with lungs of 129SvEv mice in terms of macrophage and epithelial cell localization. No expression of spike was shown in livers of 129SvEv mice.

in these experiments were generated in rabbits as follows. Gel-purified glutathione-*S*-transferase fusions of the S1 domain, the S2 domain, or the full-length spike glycoprotein (250 μg each) were mixed with Titermax and injected intramuscularly into rabbits that were later given a booster with another 125 μg of spike protein. Sera from six rabbits (two for each form of spike) were pooled. The sera were mixed and used at a dilution of 1:1,000 each. Sections were treated with trypsin (10 min at 37°C with Digest-All from Zymed) before incubation with antibodies. To detect bound antibodies, an ABC Elite kit (Vector Laboratories) was used, which employs biotinylated secondary antibodies followed by avidin-peroxidase complexes and diaminobenzidine as a chromogen. Sections were slightly counterstained with hematoxylin to show nuclei. (A, B, and C) Lung harvested on day 3 (40× lens objective). (D) Liver harvested on day 22 showing an inflammatory nodule (4× lens objective). A 40× lens objective view of a section within the nodule is shown in the inset. (E) Representative section of spleen from a day-22 animal (40× lens objective). Similar distribution of spike expression was noted in lungs of 129SvEv mice. No expression of spike was found in spleens and livers of 129SvEv mice. Lung tissues were also analyzed for specific inflammatory cells. Stat1$^{-/-}$ mice were necropsied 5 (F and H) and 22 (G and I) days after SARS CoV challenge and analyzed for expression of the T-cell marker CD3 (F and G) and the macrophage marker F4/80 (H and I) by using immunohistochemical analyses with a peroxidase-conjugated secondary antibody. No reaction was seen when an irrelevant primary antibody was used. Similar findings were obtained with tissues of 129SvEv mice.

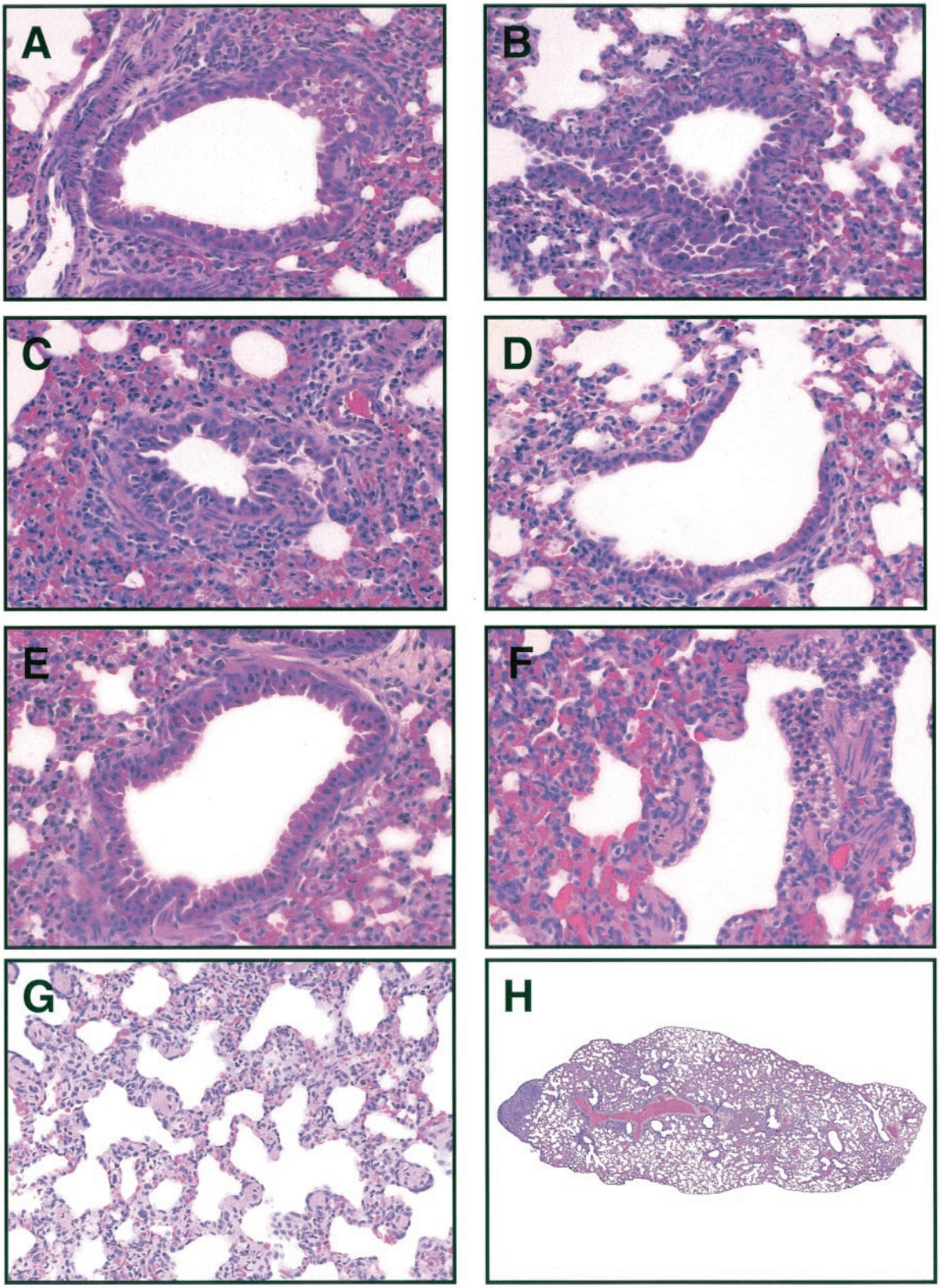

FIG. 4. Histopathology in lungs following SARS CoV challenge in 129SvEv and Stat1$^{-/-}$ mice. (A to D) Histologic sections of lungs from 129SvEv animals harvested on days 1 (A), 3 (B), 5 (C), and 22 (D) after SARS CoV challenge. All sections were viewed at an original magnification of ×60 and are shown at a magnification of ×54. (E to H) Histologic sections of lungs from Stat1$^{-/-}$ animals harvested on days 1 (panel E; original magnification, ×60; present magnification, ×54), 6 (panel F; original magnification, ×60; present magnification, ×54), 10 (panel G; original magnification, ×40; present magnification, ×36), and 15 (panel H; original magnification, ×2; present magnification, ×1.8) after SARS CoV challenge.

disease in Stat1$^{-/-}$ mice began as described for 129SvEv mice; however, progression to diffuse interstitial pneumonia with focal airspace consolidation was observed. Mild peribronchiolar mononuclear inflammation observed on day 1 (Fig. 4E) progressed to acute bronchiolitis with abundant peribronchiolar macrophages (Fig. 2H) and interstitial pneumonia on days 6 to 10 (Fig. 4F and G) despite striking sparing of airspaces (Fig. 4G). A low-magnification view of lung tissue at day 15 shows the diffuse nature of the disease, with bridging infiltrates emanating from bronchioles with subpleural consolidation (Fig. 4H). The inflammatory process progressed with infiltration of T cells throughout the lungs (Fig. 2G) and diminution of peribronchiolar macrophages (Fig. 2I); inflammation eventually extended into the anterior mediastina (data not shown). The Stat1$^{-/-}$ mice progressively lost weight (data not shown). Expression of SARS CoV antigens was noted within cells of the inflammatory pulmonary infiltrates (Fig. 2C). Livers of Stat1$^{-/-}$ mice harvested at day 22 demonstrated nodules of dense mononuclear inflammation containing SARS CoV-infected cells (Fig. 2D); the identity of these infected cells is unclear, although they were not macrophages (Fig. 3E and F). The architecture of the spleens remained normal in Stat1$^{-/-}$ mice, although SARS CoV-infected cells appeared at late time points (Fig. 2E).

Our studies clearly demonstrate replication of SARS CoV in mice following intranasal inoculation, and this finding is consistent with those in two recent reports (12, 16). Our observation of bronchiolitis in both 129SvEv mice and Stat1$^{-/-}$ mice with resolution in the former and progression to interstitial pneumonia and mediastinitis in the latter parallels the histopathology described in postmortem examination of humans who died from SARS. Although the 24 human cases studied demonstrated only diffuse alveolar damage, with edema, pneumocyte necrosis, and hyaline membrane formation or organization depending on the duration of illness before death (1, 3, 9, 15), the most detailed study led by expert pulmonary pathologists also noted bronchiolar disease with respiratory epithelial cell necrosis, loss of cilia, and intrabronchiolar fibrin deposits (3). In fact, early diffuse alveolar damage is thought to start at the level of the respiratory bronchioles, irrespective of the etiology. Thus, although the pathology noted in the mouse models may appear quite different from that in humans in that intra-alveolar edema, pneumocyte necrosis, or hyaline membranes were not observed in mice, one should not understate the common finding of bronchiolar injury with focal respiratory epithelial cell necrosis. The progression of the mice to interstitial pneumonia without development of diffuse alveolar damage may reflect real species-specific differences in host responses. Similarly, not all humans exposed to SARS CoV develop SARS. It is also possible that diffuse alveolar damage in humans is preceded by fulminate bronchiolitis but that histologic tissue examination from the first three days of illness has not yet been reported.

The mechanism by which Stat1-deficient signaling compromises the ability of the animals to clear SARS CoV infection remains unclear. A likely explanation is the abnormality in interferon activity that characterizes these animals (2, 8). In fact, data generated in our laboratory and the laboratories of others suggest that alpha/beta interferons strongly inhibit the replication of SARS CoV in vitro (5, 11a). Indeed, SARS CoV-infected macaques treated with interferon shed less virus (4). The results for the Stat1$^{-/-}$ animals highlight the importance of innate immunity in controlling SARS CoV infection and suggest potential therapeutic strategies that augment the innate immune response in the context of interferon action.

This work was funded by Southern Research Institute and GlaxoSmithKline Pharmaceuticals.

REFERENCES

1. **Ding, Y., H. Wang, H. Shen, Z. Li, J. Geng, H. Han, J. Cai, X. Li, W. Kang, D. Weng, Y. Lu, D. Wu, L. He, and K. Yao.** 2003. The clinical pathology of severe acute respiratory syndrome (SARS): a report from China. J. Pathol. **200:**282–289.
2. **Durbin, J. E., R. Hackenmiller, M. C. Simon, and D. E. Levy.** 1996. Targeted disruption of the mouse Stat1 gene results in compromised innate immunity to viral disease. Cell **84:**443–450.
3. **Franks, T. J., P. Y. Chong, P. Chui, J. R. Galvin, R. M. Lourens, A. H. Reid, E. Selbs, C. P. McEvoy, C. D. Hayden, J. Fukuoka, J. K. Taubenberger, and W. D. Travis.** 2003. Lung pathology of severe acute respiratory syndrome (SARS): a study of 8 autopsy cases from Singapore. Hum. Pathol. **34:**743–748.
4. **Haagmans, B. L., T. Kuiken, B. E. Martina, R. A. Fouchier, G. F. Rimmelzwaan, G. Van Amerongen, D. Van Riel, T. De Jong, S. Itamura, K. H. Chan, M. Tashiro, and A. D. Osterhaus.** 2004. Pegylated interferon-alpha protects type 1 pneumocytes against SARS coronavirus infection in macaques. Nat. Med. **10:**290–293.
5. **Hensley, L. E., E. A. Fritz, P. B. Jahrling, C. L. Karp, J. W. Huggins, and T. W. Geisbert.** 2004. Interferon-b 1a and SARS coronavirus replication. Emerg. Infect. Dis. **10:**317–319.
6. **Krijnse-Locker, J., M. Ericsson, P. J. Rottier, and G. Griffiths.** 1994. Characterization of the budding compartment of mouse hepatitis virus: evidence that transport from the RER to the Golgi complex requires only one vesicular transport step. J. Cell Biol. **124:**55–70.
7. **Ksiazek, T. G., D. Erdman, C. S. Goldsmith, S. R. Zaki, T. Peret, S. Emery, S. Tong, C. Urbani, J. A. Comer, W. Lim, P. E. Rollin, S. F. Dowell, A. E. Ling, C. D. Humphrey, W. J. Shieh, J. Guarner, C. D. Paddock, P. Rota, B. Fields, J. DeRisi, J. Y. Yang, N. Cox, J. M. Hughes, J. W. LeDuc, W. J. Bellini, and L. J. Anderson.** 2003. A novel coronavirus associated with severe acute respiratory syndrome. N. Engl. J. Med. **348:**1953–1966.
8. **Meraz, M. A., J. M. White, K. C. Sheehan, E. A. Bach, S. J. Rodig, A. S. Dighe, D. H. Kaplan, J. K. Riley, A. C. Greenlund, D. Campbell, K. Carver-Moore, R. N. DuBois, R. Clark, M. Aguet, and R. D. Schreiber.** 1996. Targeted disruption of the Stat1 gene in mice reveals unexpected physiologic specificity in the JAK-STAT signaling pathway. Cell **84:**431–442.
9. **Nicholls, J. M., L. L. Poon, K. C. Lee, W. F. Ng, S. T. Lai, C. Y. Leung, C. M. Chu, P. K. Hui, K. L. Mak, W. Lim, K. W. Yan, K. H. Chan, N. C. Tsang, Y. Guan, K. Y. Yuen, and J. S. Peiris.** 2003. Lung pathology of fatal severe acute respiratory syndrome. Lancet **361:**1773–1778.
10. **Peiris, J. S., S. T. Lai, L. L. Poon, Y. Guan, L. Y. Yam, W. Lim, J. Nicholls, W. K. Yee, W. W. Yan, M. T. Cheung, V. C. Cheng, K. H. Chan, D. N. Tsang, R. W. Yung, T. K. Ng, and K. Y. Yuen.** 2003. Coronavirus as a possible cause of severe acute respiratory syndrome. Lancet **361:**1319–1325.
11. **Risco, C., M. Muntion, L. Enjuanes, and J. L. Carrascosa.** 1998. Two types of virus-related particles are found during transmissible gastroenteritis virus morphogenesis. J. Virol. **72:**4022–4031.

11a. **Spiegel, M., A. PIchlmair, E. Muhlberger, O. Haller, and F. Weber.** 2004. The antiviral effect of interferon-beta against SARS-coronavirus is not mediated by MxA protein. J. Clin. Virol. **30:**211–213.

12. **Subbarao, K., J. McAuliffe, L. Vogel, G. Fahle, S. Fischer, K. Tatti, M. Packard, W. J. Shieh, S. Zaki, and B. Murphy.** 2004. Prior infection and passive transfer of neutralizing antibody prevent replication of severe acute respiratory syndrome coronavirus in the respiratory tract of mice. J. Virol. **78:**3572–3577.
13. **Thiel, V., K. A. Ivanov, A. Putics, T. Hertzig, B. Schelle, S. Bayer, B. Weissbrich, E. J. Snijder, H. Rabenau, H. W. Doerr, A. E. Gorbalenya, and J. Ziebuhr.** 2003. Mechanisms and enzymes involved in SARS coronavirus genome expression. J. Gen. Virol. **84:**2305–2315.
14. **Tooze, J., S. A. Tooze, and S. D. Fuller.** 1987. Sorting of progeny coronavirus from condensed secretory proteins at the exit from the trans-Golgi network of AtT20 cells. J. Cell Biol. **105:**1215–1226.
15. **Tse, G. M., K. F. To, P. K. Chan, A. W. Lo, K. C. Ng, A. Wu, N. Lee, H. C. Wong, S. M. Mak, K. F. Chan, D. S. Hui, J. J. Sung, and H. K. Ng.** 2004. Pulmonary pathological features in coronavirus associated severe acute respiratory syndrome (SARS). J. Clin. Pathol. **57:**260–265.
16. **Yang, Z. Y., W. P. Kong, Y. Huang, A. Roberts, B. R. Murphy, K. Subbarao, and G. J. Nabel.** 2004. A DNA vaccine induces SARS coronavirus neutralization and protective immunity in mice. Nature **428:**561–564.